HOSTED BY

ELSEVIER

CrossMark

Available online at www.sciencedirect.com

ScienceDirect

Progress in Natural Science: Materials International 25 (2015) 131–136

Progress in Natural Science Materials International

www.elsevier.com/locate/pnsmi
www.sciencedirect.com

Original Research

Structural and spectroscopic analysis of wurtzite $(ZnO)_{1-x}(Sb_2O_3)_x$ composite semiconductor

Hafeez ullah[a,b,*], Amjid Iqbal[c], M. Zakria[c], Arshad Mahmood[c]

[a]University of Trento, Department of Physics, Via Sommarive 14, Povo, 38123 Trento, Italy
[b]Center for Materials and Microsystems, Fondazione Bruno Kessler, Via Sommarive 18, Povo, 38123 Trento, Italy
[c]National Institute of Lasers and Optronics (NILOP), Nilore, Islamabad, Pakistan

Received 9 August 2014; accepted 29 September 2014
Available online 12 May 2015

Abstract

The structural, vibrational and impedance analysis for $(ZnO)_{1-x}(Sb_2O_3)_x$ composite synthesized by solid state reaction technique were carried out in the present investigation. X-ray diffraction (XRD) study showed that $(ZnO)_{1-x}(Sb_2O_3)_x$ composite has hexagonal (wurtzite) crystal structure. Variation in lattice constants with Sb-doping indicated the proper incorporation of Sb dopant in ZnO host matrix. The results of Raman spectroscopy test suggested the signature of E_2 (high) and E_1 (TO) Raman modes, and verified the wurtzite structure of $(ZnO)_{1-x}(Sb_2O_3)_x$ composite. Two additional phonon bands (671, 712) cm^{-1} appeared in Raman spectra of composite samples due to the existence of the lattice defects caused by Sb doping or may be other intrinsic lattice defects formed during the synthesis of $(ZnO)_{1-x}(Sb_2O_3)_x$ composite. The frequency dependent on the electrical characteristics, such as, impedance (Z), dielectric constant (ε) and AC conductivity (σ) have been studied in a range of frequencies for different Sb concentration at room temperature. The electrical measurement results showed that the impedance increased with Sb dopant concentration, while dielectric constant and AC conductivity decreased with Sb dopant concentration.

Keywords: $(ZnO)_{1-x}(Sb_2O_3)_x$; Semiconductors; XRD; Raman spectroscopy; Impedance spectroscopy

1. Introduction

ZnO is a group II–VI direct wide band gap semiconductor materials ($E_g = 3.37$ eV at room temperature) with large exciton binding energy (60 meV), making it to be a promising material for optoelectronic applications such as light emitting diodes (LED), field effect transistors, lasers diodes, and photo detectors [1–5]. It is well known that doping with proper element is an effective technique to manipulate structural and optical properties of the wide band gap semiconductor materials. The doping of ZnO may provide us with a material having versatile characteristics. Metal oxide doped ZnO are the multifunctional materials with co-existing optical, magnetic, semiconducting and electromechanical properties which provides an avenue for scientific exploration [6]. Undoped ZnO exhibit n-type behavior due to intrinsic defects, which make it very difficult to obtain p-type ZnO because of the "self-compensation" resulting from the donor defects such as Zn interstitials, oxygen vacancies or hydrogen impurities generated during crystal growth environment [7,8]. p-Type ZnO are absolutely required for effective light emitting diode (LED) device fabrication and the reliable p-type doping of ZnO is an obstacle for wide range of applications in photonics and electronics devices [9]. To achieve p-type doping a range of doping techniques have been applied and investigated. Various p-type dopant elements of group I (K, Li, Na) and group V (N, P, Cu, Ag, As) have been used [10–12]. However, good device performance has not observed yet. Antimony (Sb) is a useful group V dopant element owing to its close ionic radii Sb^{3+}

*Corresponding author at: Department of Physics, University of Trento, Via Sommarive 14, Povo, 38123 Trento, Italy. Tel.: +39 461 281504.
E-mail address: Hafeezullah83@gmail.com (H. ullah).
Peer review under responsibility of Chinese Materials Research Society.

http://dx.doi.org/10.1016/j.pnsc.2015.02.003

(.076 nm) with Zn^{2+} (.074 nm) and tune-ability of structural, optical and electrical properties of ZnO [13]. Theoretical calculation shows that Sb doping in ZnO can generate shallow acceptor levels in ZnO, if Sb atom substitutes Zn atom and connect with two Zn vacancies [14]. In this way, various Sb-doped ZnO composite have been prepared to investigate different features of the target samples by using X-ray diffraction (XRD), Raman and impedance spectroscopy. Raman spectroscopy is a powerful and nondestructive technique to elaborate impurity-induced modes and their concentrations effect on Raman peaks. Sb with $5s^25p^3$ electronic configuration is expected to modify the structural and electrical properties of ZnO. However, the structural and optical properties of this material have been rarely reported. This motivates us to study Sb-doped ZnO properties in bulk forms. In this work, we have prepared $(ZnO)_{1-x}(Sb_2O_3)_x$ composite samples using the technique of solid state reaction. Our efforts were concentrated on the structural, optical phonon scattering and electrical characterizations to manifest the changes appear in ZnO due to Sb doping as well as the competency of this material for optoelectronics applications [15].

2. Experimental details

High analytical grade ZnO and Sb_2O_3 powder were used to prepare $(ZnO)_{1-x}(Sb_2O_3)_x$ ($x=0$, 1.5,2, 3, 5) composite. Different composition of ZnO (98.5, 98, 97 and 95 mol%) and Sb_2O_3 (1.5, 2, 3 and 5 mol%) were mixed by pestal and mortar for 3 h to make solid solution. The mixtures were pressed to form pellets and sintered at 1000 °C for 3 h in air to avoid oxygen deficiency and to make proper incorporation of Sb through Zn lattice sites. The synthesized samples have been subjected to XRD, Raman and impedance spectroscopy for structural, vibrational and electrical characterization. XRD analysis have been carried out by a Bruker D-8, X-ray diffractometer equipped with a Cu*K*α-radiation ($\lambda=1.54186$ Å). The measurements carried out by $\theta/2\theta$ scans in the 2θ angular range of 20–80°, with a step size of 0.02° and a scan rate of 2°/min. Raman spectroscopy have been performed with the help of Dongwoo Optron MST-4000A Raman spectrometer of 532 nm He–Cd laser source. Electrical properties have been determined by impedance spectroscopy with Alpha high frequency analyzer and Novocontrol sample holder at room temperature. Silver electrodes were used to connect the pellets to the instrument.

3. Results and discussion

3.1. X-ray diffraction analysis

XRD analysis were used to examine the crystal structure, crystallinity and plane orientation of the $(ZnO)_{1-x}(Sb_2O_3)_x$ composite. Fig. 1 shows that the crystal structure is hexagonal (wurtzite) for all diffraction peaks that can be indexed to the peaks of ZnO wurtzite structure (JCPDS 79-2205). The XRD spectra show that the crystal structure is single phase with no impurity peak of Sb or its oxide up-to 3 mol% Sb_2O_3 dopant concentration. However, for 5 mol% of Sb_2O_3 the XRD peaks corresponding to the $Zn_7Sb_2O_{12}$ (JCPDS 74-1858) phase were observed, which indicates that the structure shift from mono phase to heterophase.

The lattice spacing for all the samples was calculated using Bragg's relation:

$$d = \lambda/(2\ \sin\ \theta) \tag{1}$$

where θ is the angle between normal to diffracting plane and incident X-ray, λ is the wavelength of X-rays, which is in our case was Cu*K*α radiation having wavelength 1.5405 Å. The lattice parameters have been calculated using the following expression for hexagonal system [16,17].

$$\frac{1}{d^2} = \frac{4}{3}\left(\frac{h^2+hk+k^2}{a^2}\right) + \frac{l^2}{c^2} \tag{2}$$

The lattice parameters a and c calculated for different samples are shown in Table 1. The lattice constants calculated from XRD pattern for pure ZnO and composite samples are nearly equal to the lattice constants given in the standard data (JCPDS, 79-2205, 80-0075). There is a little increase in lattice parameters with respect to dopant concentration, which is due to incorporation of Sb ion at the Zn lattice sites. The change in the lattice parameters of ZnO host material depends on the ionic radii of the impurity that substitute the Zn ions at the lattice site. In case of Sb doping the ionic radii of the Sb^{3+} (.076 nm) is larger than Zn^{2+} (.074 nm). If Sb^{3+} ion substitutes Zn^{2+} ion in ZnO host lattice, then the variation in the lattice constants is expected due to ionic radii difference which has also been reported elsewhere [18]. The small improvement in the lattice parameters with doping concentration, leads to believe that some of Sb^{3+} ions have substituted Zn^{2+} ions in ZnO lattice. The average crystallite size D is calculated using the Sherrer's formula [16]:

$$D = \frac{0.9\lambda}{\beta\ \cos\ \theta} \tag{3}$$

where D is the crystallite size, λ is X-ray wavelength, β is full width at half maxima and θ is Bragg's angle in radian. The average crystallite size (Table 1) has been decreased with the variation in Sb doped concentration. The decrease of crystallite size give arises to a developed surface with large boundaries leading to larger scattering phenomena, which in turn affects the carrier's mobility. Thus, a resistivity increase is expected from Sb doped samples. For further investigation, the crystallite size (D) and Stoke–Wilson equation was used to calculate the dislocation density (δ) as follow [19]:

$$\delta = \frac{15}{aD}\left(\frac{\lambda}{D\ \cos\ \theta} - \beta\right)\frac{1}{\tan\ \theta} \tag{4}$$

where D is the crystallite size in nm, a is the lattice constant and β is the full width at half maxima. The dislocation density value increases from 2.67×10^{15} to $4.62\times10^{15}/m^2$ with Sb concentration.

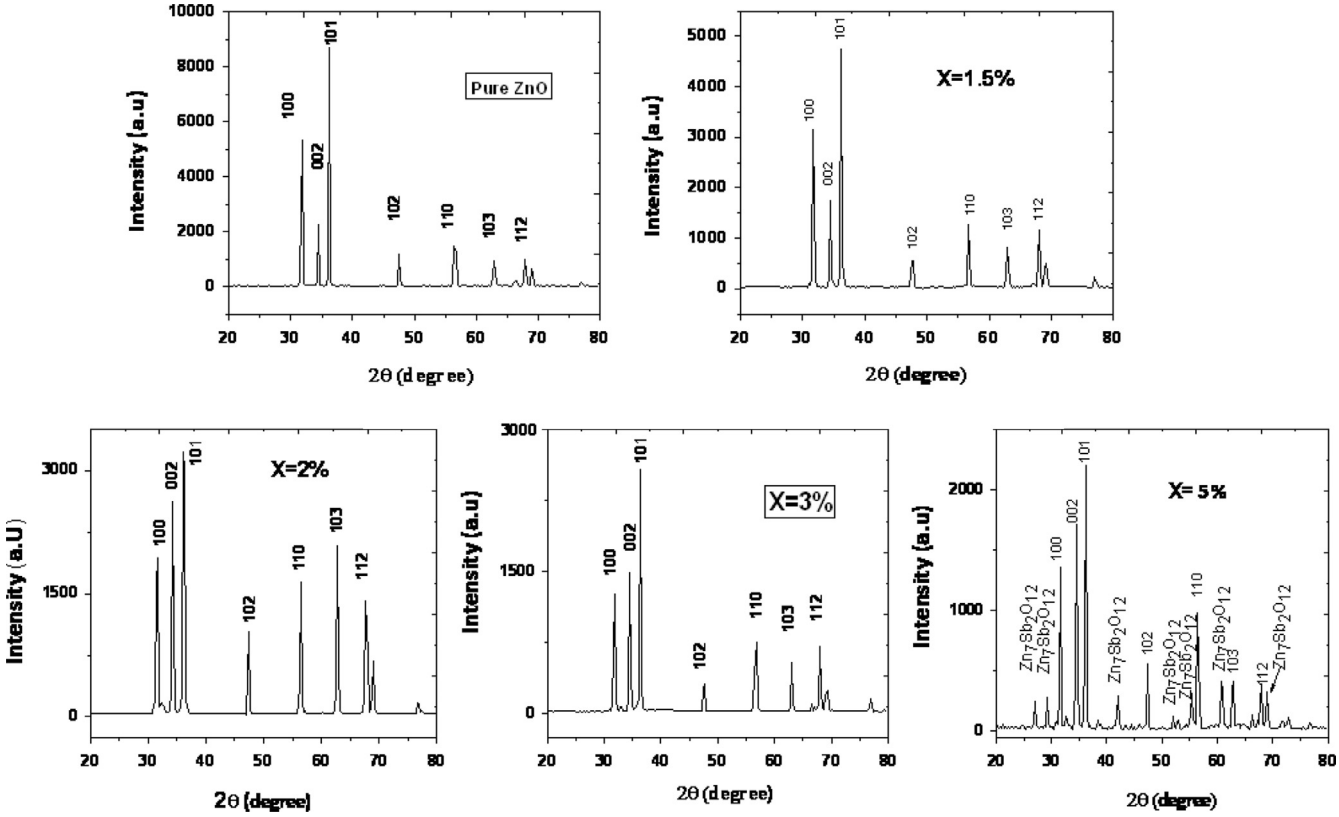

Fig. 1. X-ray diffraction (XRD) patterns of $(ZnO)_{1-x}(Sb_2O_3)_x$ composite sintered at 1000 °C.

Table 1
Lattice parameters a and c calculated for different samples.

S. nos.	Sb_2O_3 composition (x) (mol%)	Lattice constant c (nm)	Lattice constant a (nm)	Crystallite size (nm)	Dislocation density δ (m^{-2})
(1)	0	0.52076	0.32547	31.65	2.67×10^{15}
(2)	1.5	0.52081	0.32550	29.72	3.26×10^{15}
(3)	2	0.52086	0.325538	27.80	3.95×10^{15}
(4)	3	0 .52087	0.32554	24.30	4.62×10^{15}
(5)	5	0.52127	0.32579	21	4.16×10^{15}

3.2. Raman spectroscopy

Raman spectroscopy is a powerful tool to analyze the crystalline quality, structural faults, and defects in the target materials. The wurtzite ZnO $P6_3mc$ belongs to the space group with six Raman active optical phonon modes in the center of the Brillouin zone as $\Gamma_{opt}=2A_1+2E_1+2E_2$, where E_1, E_2 and A_1 are first-order Raman-active mode [20,21]. The E_1 and A_1 polar modes split into longitudinal optical (LO) and transverse optical (TO) components, while the E_2 non-polar modes (low and high) are Raman active. The measured Raman spectra of ZnO and $(ZnO)_{1-x}(Sb_2O_3)_x$ composite in the range 200–800 cm^{-1} is shown in Fig. 2. In pure ZnO, peaks at 330, 380, 436 cm^{-1} have been appeared in the low wave number region. The same Raman peaks were detected for

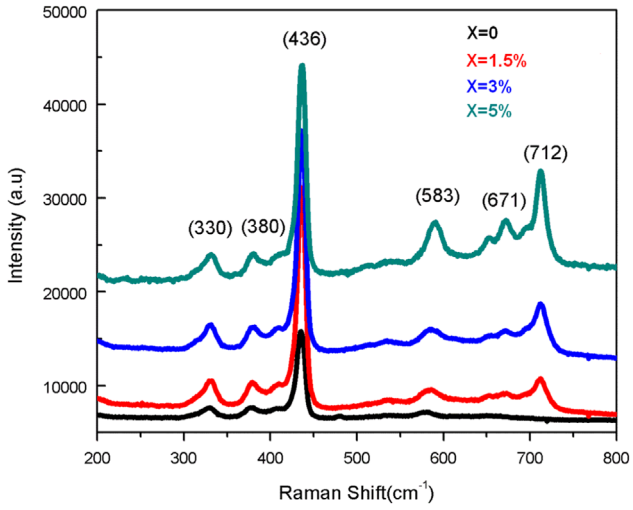

Fig. 2. Raman spectra of the $(ZnO)_{1-x}(Sb_2O_3)_x$ ($x=0$, 1.5, 3, 5) composite sintered at 1000 °C.

$(ZnO)_{1-x}(Sb_2O_3)_x$ bulk, but with higher intensities. In addition, peaks at 671 and 712 cm^{-1} were found in the high wave number regime for composite samples. In the low wave number region, the peak at 330 cm^{-1} is related to multiphoton process and has been assigned as E_2 (high)–E_2 (Low) arising from zone boundary phonons [22]. Peak at 380 cm^{-1} corresponds to A_1 (TO) mode, which arises due to some defects like Zn interstitials, oxygen vacancies and also their complexes

[23,24]. One of the sharp and remarkable peaks at 436 cm^{-1} was detected for all samples and assigned as E_2 (high) mode. This is the strongest mode in wurtzite crystal structure and is due to the motion of oxygen atoms in ZnO lattice [25]. The location of the E_2 (high) mode shows no obvious change with increase in Sb contents, but intensity enhanced with Sb doping level. In the regime of high Raman shift, a peak appears at 583 cm^{-1} for all samples, whose intensity increases gradually with Sb doping and it is the signature of the E_1 (LO) mode [26]. Similar effects have been investigated in the literature reviews for various doping impurities interpreted as an indication of oxygen deficiency [27–29]. Two additional modes at 671, 712 cm^{-1} have been found in $(ZnO)_{1-x}(Sb_2O_3)_x$ samples. These modes become prominent as the doping concentration of Sb in ZnO increases. Moreover, when doping ion occupies the Zn sites, lattice or intrinsic host-lattice defects are activated, leading to additional vibration modes. Therefore, these modes may show the presence of the ZnO lattice defects that might be caused by Sb or other intrinsic lattice defects.

3.3. Impedance spectroscopy

3.3.1. Impedance analysis

The AC electrical behavior of bulk $(ZnO)_{1-x}(Sb_2O_3)_x$ composite was studied over a range of frequencies by using complex impedance spectroscopy. Impedance data having capacitive and resistive components is plotted and shown (in Fig. 3) in the form of semicircular arc representing electrical phenomenon due to bulk (grain) material, grain boundary and interfacial phenomenon, if any. Generally, the grains are effective in high frequency region while the grain boundaries are effective in low frequency region [30]. Fig. 3 shows the Nyquist plots of $(ZnO)_{1-x}(Sb_2O_3)_x$ composite at different dopant concentrations. It is evident that all the samples show single semicircular arc excluding ($x=2$ mol%) ZnO, which implies that grain boundary resistance contribution, affects the total impedance with the addition of grain resistance in this sample. The first semicircle occurring in the high frequency region corresponds to grain resistance while the second in the low frequency region corresponds to grain boundaries. This can be attributed to the decrease in grain size as a result of doping. In literature it has been reported that the resistivity of a polycrystalline material, in general, increases with the decrease in grain size as depicted in XRD [31,32]. Accordingly, smaller grains imply a larger number of insulating grain boundaries which act as a barrier to the flow of electrons. Smaller grains also imply smaller grain–grain surface contact area and, therefore, a reduced electron flow. The grain size decreasing with increasing dopant concentration resulting in more number of grain boundaries in doped samples. Therefore, the grain boundary contribution becomes dominant and grain contribution is not resolved for ($x=3$ mol%) sample and appears as one semicircle. Moreover, the incorporation of Sb in ZnO system increases the concentration of defect ions which tend to segregate at grain boundaries leading to the formation of grain boundary defect barriers [33]. The dopant concentration increases barrier height increases which directly increase the resistivity (impedance) [34] as revealed by Fig. 3.

3.3.2. Dielectric analysis

Fig. 4 shows that the dielectric constant decreases with the increase in frequency and becomes almost invariable at high frequencies for all composition. This behavior can be elucidated by Maxwell–Wagner interfacial model [35]. In this model, the dielectric medium is considered to be composed of two layers, conducting grains which are separated by resistive grain boundaries. Under the application of external electric field, the charge carriers can easily conduct within grains but are accumulated at the grain boundaries. This process can create large polarization which results high dielectric constant. Moreover, the higher value of dielectric constant can also be explained on the basis of interfacial/space charge polarization due to inhomogeneous dielectric structure. And the in homogeneity may be attributed to the porosity and

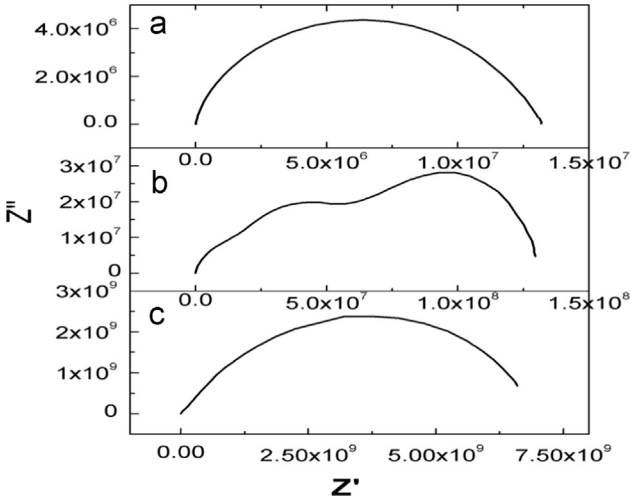

Fig. 3. Impedance spectra (Nyquest plot) of $(ZnO)_{1-x}(Sb_2O_3)_x$ composite (a) $x=1.5\%$ (b) $x=2\%$ (c) $x=3\%$.

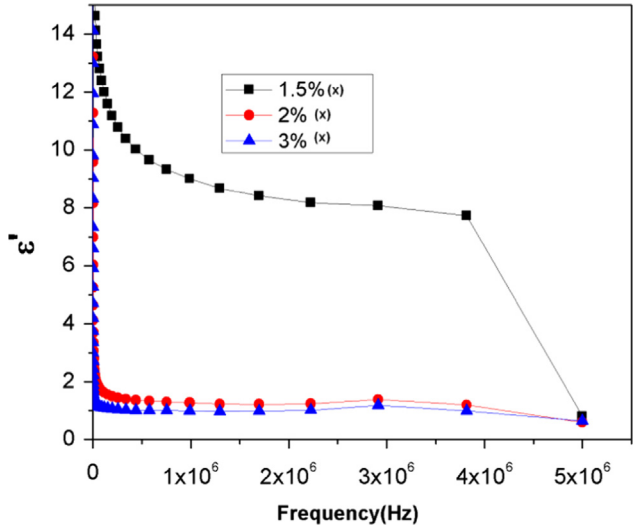

Fig. 4. Variation of dielectric constant ε' vs. frequency and dopant concentrations.

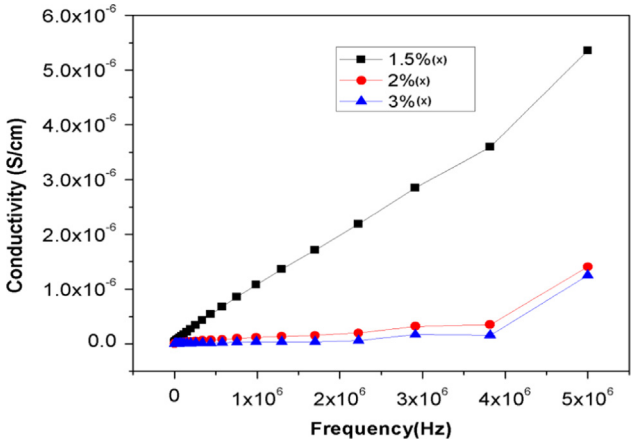

Fig. 5. AC conductivity (σ) vs. frequency (f) for different Sb doping concentration of $(ZnO)_{1-x}(Sb_2O_3)_x$ composite.

structure of the grains. The polarization (dielectric constant) decreases with the increase in frequency and then maintains a constant value owing to the fact that beyond a specific frequency of AC field the hopping of Sb ions cannot pursue the AC field. It has also been revealed that the value of dielectric constant decreases with the increase in Sb dopant concentration. It may be due to the small dielectric polarizability of Sb ions compared to Zn [36]. Consequently, as the dopant concentration increases more Zn ions will be replaced by Sb ions and thus decreasing the polarization, which in turn decreases the dielectric constant.

3.3.3. *AC conductivity*

The frequency dependent conductivity is a powerful technique for studying the hopping dynamics of the charge carriers. The AC conductivity (σ) due to localized states is expressed by power law [37]:

$$\sigma_{ac}(\omega) = \sigma_0 + A\omega^n \quad (5)$$

where σ_0 is the dc part of conductivity, A is temperature dependent constant and n is a parameter depends on frequency and temperature. With increasing frequency, the AC conductivity increased and obeyed the power law. It is depicted from Fig. 5 that as the Sb_2O_3 increased; the AC conductivity became frequency-independent, with a slight increase on the higher frequency side. Thus, the corresponding conductivity was close to the dc conductivity (σ). Moreover, the values of exponent lying between 0 and 1 implies that slope of the curve are less than 1. This suggests that the conduction mechanism is corresponding to the translational hopping motion with successful hops of carriers/ions [38]. It is shown from Fig. 5 that the AC conductivity decreases as Sb concentration increases at room temperature, which is attributed to the crystallite sizes effect and decreases in carrier/electrons concentration. As Sb content increases in the ZnO composite, the crystallite size decreases as shown in XRD analysis, consequently the crystallite boundaries density increases. This leads to more accumulated charge at the interfaces, results the increase in bulk resistivity [39].

4. Conclusions

In summary we have synthesized high quality $(ZnO)_{1-x}(Sb_2O_3)_x$ bulk samples by solid state reaction method and investigated their structural, vibrational and electrical properties. The analysis of XRD indicates polycrystalline wurtzite structure of ZnO along with proper incorporation of Sb^{3+} at the Zn lattice sites. The marginal increase in lattice parameters has been observed after Sb doping, indicating partial substitution in host matrix. The Raman spectroscopy reveals two additional modes at 671 and 712 cm^{-1} which are the indicative of the existence of the host lattice defects caused by Sb doping or other intrinsic lattice defects that formed during the synthesis of $(ZnO)_{1-x}(Sb_2O_3)_x$ composite. The complex impedence spectroscopy of the $(ZnO)_{1-x}(Sb_2O_3)_x$ composite samples show an increasing trend in impedance value with increase in doping concentration. Using the impedance spectroscopy the dielectric and AC conductance have been studied, and both of them follow decreasing behavior as the doping concentration increase.

Acknowledgment

The author would like to acknowledge Dr. Nasir khan, Dr. Nadeem and Ms Robeena (PINSTECH) for their help and encouragement during this work.

References

[1] Jang-Won Kang, Yong-Seok Choi, Minhyeok Choe, Na-Yeong Kim, Takhee Lee, Bong-Joong Kim, CW Tu, Seong-Ju Park, Nanotechnology 23 (2012) 495712–495716.
[2] S.Y. Lee, E.S. Shim, H.S. Kang, S.S. Pang, J.S. Kang, Thin Solid Films 473 (2005) 31–34.
[3] Z.L. Wang, X.Y. Kong, Y. Ding, P. Gao, W.L. Hughes, R. Yang, Y. Zhang, Adv. Funct. Mater. 14 (2004) 943–956.
[4] H. Harima, J. Phys.: Condens. Matter 16 (2004) S5653.
[5] R. Könenkamp, R.C. Word, C. Schlegel, Appl. Phys. Lett. 85 (24) (2004) 6004–6006.
[6] P. Wang, N. Chen, Z. Yin, F. Yang, C.J. Peng, Cryst. Growth 290 (2006) 56–60.
[7] G. Mandel, Phys. Rev. A 134 (1964) 1037.
[8] C.G. van deWalle, Phys. Rev. Lett. 85 (2000) 1012.
[9] Shashi B. Rana, Amarpal singh, Satbir Singh, Int. J. Nanoelectron. Mater. 6 (2013) 45–57.
[10] J. Wang, L. Gao, Inorg. Chem. Commun. 6 (2003) 877–881.
[11] J. Wang, L. Gao, Solid State Commun. 132 (2004) 269–271.
[12] K. Vanheusden, W.L. Warren, C.H. Seager, D.R. Tallant, J.A. Voigt, B.E. Gnade, J. Appl. Phys. 79 (1996) 7983.
[13] R.D. Shannon, Acta Crystallogr. A 32 (1976) 751–767.
[14] A. qbal, A. Mahmood, T.M. Khan, E. Ahmed, Prog. Nat. Sci.- Mater. 23 (2013) 64–69.
[15] S. Limpijumnong, S.B. Zhang, S.H. Wei, C.H. Park, Phys. Rev. Lett. 92 (2004) 155504.
[16] B.D. Cullity, Elements of X-ray Diffraction, second ed., Addison-Wesley, Reading, MA, 1978, p. 102–110.
[17] D.S. Rickerby, A.M. Jones, B.A. Bellamy, Surf. Coat. Technol. 37 (1989) 111–137.
[18] D.h. kim, N.G. Cho, K.S. kim, S. Han, H.G. Kim, J. Electroceram. 22 (2009) 82–86.
[19] T. Mahalingam, A. Kathalingam, S. Velumani, S. Lee, M.H. Sun, K.Y. Deak, J. Mater. Sci. 41 (2006) 3553–3559.

[20] T.C. Damen, S.P.S. Porto, B. Tells, Phys. Rev. 142 (1966) 570.
[21] T.M. Khan, M. Irfan, Appl. Phys. A 117 (2014) 1275–1282.
[22] J.M. Calleja, M. Cardona, Phys. Rev. B 16 (1977) 3753.
[23] C.X. Zhu, G.P. Li, X. Yang, Y. Tan, S.T. Sun, X.W. Lincoln, C. Smith, T.A, J. Appl. Phys. 103 (9) (2008) 094303.
[24] J.M. Calleja, M. Cardona, Phys. Rev. B 16 (1977) 3753.
[25] D.G. Mead, G.R. Wilkinson, J. Raman Spectrosc. 6 (1997) 123–129.
[26] Zhaochun, Z. Baibiao, H. Yongqin, Y. Deliang, Mater. Sci. Eng., B 86 (2) (2001) 109–112.
[27] C. Bundesmann, N. Ashkenov, M. Schubert, D. Spemann, T. Butz, E. M. Kaidashev, M. Lorenz, M. Grundmann, Appl. Phys. Lett. 83 (2003) 1974–1976.
[28] S.K. Sharma, G.J. Exarhos, Solid State Phenom. 55 (1997) 32–38.
[29] X.L. Xu, S.P. Lau, B.K. Tay, Thin Solid Films 398–399 (2001) 244–249.
[30] L.L. Dıaz-Flores, R. Ramirez-Bon, A. Mendoza-Galvan, E. Prokhorov, J. Gonzalez-Hernandez, J. Phys. Chem. Solids 64 (2003) 1037–1042.
[31] G.C. Kuezynski, N.A. Hooton, C.F. Gibbon, Sintering and Related Phenomenon, Gordon and Breach, New York, NY, 1967, p. 65.
[32] M. Pal, P. Brahma, D. Chakravorthy, J. Phys. Soc. Jpn. 63 (1994) 3356–3360.
[33] C. Li, J. Wang, W. Su, H. Chen, W. Zhong, P. Zhang, Ceram. Int. 27 (2001) 655–659.
[34] R. Parra, J.A. Varela, C.M. Aldao, M.S. Castro, Ceram. Int. 31 (2005) 737–742.
[35] T. Prodromakis, C. Papavassiliou, Appl. Surf. Sci. 255 (2009) 6989–6994.
[36] R.D. Shannon, J. Appl. Phys. 73 (1993) 348–366.
[37] Dhananjay, J. Nagaraju, S.B. Krupanidhi, J. Appl. Phys. 101 (2007) 104104–104104-7.
[38] Moti Ram, S. Chakrabarti, J. Alloys Compd. 462 (2008) 214–219.
[39] Ala eddin A. Saif, P. Poopalan, J. Mater. Sci. Technol. 27 (2011) 802–808.